Eur J Nucl Med Mol Imaging (2015) 42:562–578
DOI 10.1007/s00259-014-2979-0

REVIEW ARTICLE

Functional MRI and CT biomarkers in oncology

J. M. Winfield · G. S. Payne · N. M. deSouza

Received: 11 December 2014 / Accepted: 15 December 2014 / Published online: 13 January 2015

Abstract Imaging biomarkers derived from MRI or CT describe functional properties of tumours and normal tissues. They are finding increasing numbers of applications in diagnosis, monitoring of response to treatment and assessment of progression or recurrence. Imaging biomarkers also provide scope for assessment of heterogeneity within and between lesions. A wide variety of functional parameters have been investigated for use as biomarkers in oncology. Some imaging techniques are used routinely in clinical applications while others are currently restricted to clinical trials or preclinical studies. Apparent diffusion coefficient, magnetization transfer ratio and native T_1 relaxation time provide information about structure and organization of tissues. Vascular properties may be described using parameters derived from dynamic contrast-enhanced MRI, dynamic contrast-enhanced CT, transverse relaxation rate (R_2*), vessel size index and relative blood volume, while magnetic resonance spectroscopy may be used to probe the metabolic profile of tumours. This review describes the mechanisms of contrast underpinning each technique and the technical requirements for robust and reproducible imaging. The current status of each biomarker is described in terms of its validation, qualification and clinical applications, followed by a discussion of the current limitations and future perspectives.

Keywords MRI · CT · Biomarker · Oncology

J. M. Winfield · G. S. Payne · N. M. deSouza
CRUK Imaging Centre at the Institute of Cancer Research, Institute of Cancer Research and Royal Marsden NHS Foundation Trust, Sutton, UK

J. M. Winfield (✉)
MRI Unit, Institute of Cancer Research and Royal Marsden Hospital, Downs Road, Sutton SM2 5PT, UK
e-mail: jessica.winfield@icr.ac.uk

Introduction

The delivery of personalized medicine demands the availability of robust and reliable biomarkers. Although these may be genetic, serum or functional imaging parameters, only the last of these have the capacity to provide information on change through the course of the disease and on disease heterogeneity both among and within lesions. Thus, imaging biomarkers are invaluable in providing information not just for diagnostic purposes at the outset, but also on informing clinical decision-making at various points in a treatment pathway.

The availability of functional imaging biomarkers has superseded the traditional concept of imaging as a purely morphological tool that provides information on the size or volume change of a tumour with time and treatment. Aspects of a tumour such as its changing vascular profile, water content, degree of apoptosis or necrosis or metabolism are all now measurable through advanced imaging techniques using magnetic resonance imaging (MRI), computed tomography (CT) and radioisotope studies with SPECT and PET. Techniques such as dynamic contrast-enhanced (DCE) imaging allow derivation of semi-quantitative parameters (such as the enhancement fraction), but pharmacokinetic modelling allows estimation of quantitative parameters such as permeability and wash-out. Likewise, diffusion-weighted MRI (DW MRI) provides information about the cellularity of tumours, as well as the change in the extracellular water compartment in the face of increasing apoptosis or necrosis. MR spectroscopy interrogates metabolite levels within tumours and their relative changes with tumour evolution and treatment. This review focuses on the functional techniques currently available in the clinic with MRI and CT, and explores the difficulties and limitations in measurement that need to be addressed for successful implementation of the imaging biomarker in a clinical setting.

The tissue organization, vascular and metabolic biomarkers discussed in this article are summarized in Table 1.

Tissue organization biomarkers

Apparent diffusion coefficient

Mechanisms of contrast DW MRI exploits the incoherent motion of water molecules within tissues to generate contrast. Many solid tumours exhibit restricted diffusion of water molecules compared to many normal tissues, leading to bright signal on diffusion-weighted images and low values of apparent diffusion coefficient (ADC) [1, 2].

Following the initial radiofrequency (RF) excitation, two or more diffusion-encoding gradients are applied along a specified direction, separated by a refocusing RF pulse. The diffusion-encoding gradients induce a loss of phase coherence, and hence loss of signal, of the protons which have moved in the direction of the gradient during the diffusion encoding time (typically a few tens of milliseconds). The diffusion-weighted images show lower signals from voxels where the water molecules diffuse freely and higher signals from voxels where diffusion of water molecules is more restricted.

The strength of the diffusion-weighting is determined by the magnitudes and timings of the diffusion-weighting gradients and is commonly described by a summary parameter known as the b-value [3]. Estimates of ADC may be derived from fitting a monoexponential function to the signal (S) measured at two or more b-values (Eq. 1).

$$S(b) = S_0 \exp(-b.ADC) \quad (1)$$

Restricted diffusion within tumours has been shown to be related to increased cellularity and reduction in extracellular space [1, 2, 4]. Increases in necrosis and cell death after treatment increases ADC [1, 2], which has been shown to be predictive of response to chemotherapy in various tumour sites [4, 5].

Technical requirements DW MRI can be carried out on most modern MR scanners and does not require administration of exogenous contrast agents. Echoplanar imaging (EPI) is usually employed to reduce sensitivity to motion [3]. EPI is, however, sensitive to field inhomogeneities and chemical shift artefacts and optimization of sequence parameters is required to obtain good quality images [6]. Good B_0 homogeneity, minimal eddy current effects, high signal-to-noise ratio (SNR) and good fat suppression are required [6]. ADC maps are provided by the manufacturers' software. Many studies

Table 1 Tissue organization, vascular and metabolic biomarkers discussed in this article

	Biomarker	Mechanism/biology	Imaging platform	Stage of development
Tissue organization	Apparent diffusion coefficient (ADC)	Diffusion of water molecules	MR	Clinical applications, clinical trials, multicentre studies, preclinical studies, ongoing validation and qualification [6, 7, 10, 12 14, 21, 30]
	Magnetization transfer ratio (MTR)	Transfer of magnetization from bound pool to free pool	MR	Small numbers of preclinical and clinical studies, requires validation and qualification [35, 39, 44]
	Longitudinal relaxation time (native T_1)	Local environment of water molecules	MR	Preclinical studies, small number of clinical studies, requires validation and qualification [51, 56, 57]
Vascular	K^{trans} and IAUGC from DCE MRI	Structure and function of microvessels	MR	Clinical trials, multicentre studies, preclinical studies, ongoing validation and qualification [55, 68, 71, 72, 75]
	BF, BV, MTT, PS and FE product from DCE CT	Structure and function of microvessels	CT	Clinical applications, clinical trials, multicentre studies, preclinical studies, ongoing validation and qualification [66, 77, 80, 81, 83–85]
	Transverse relaxation rate (R_2*)	Local environment of water molecules; presence of paramagnetic species	MR	Preclinical studies, small number of clinical studies, requires validation and qualification [88–90, 92, 93]
	Vessel size index (VSI)	Average vessel diameter	MR	Preclinical studies, small number of clinical studies, requires validation and qualification [97, 99–101]
	Relative blood volume (rBV)	Proportion of voxel occupied by blood	MR	Preclinical studies, clinical studies in brain, small number of extracranial clinical studies, requires validation and qualification [97, 110, 117]
Metabolic	Ratios of peak areas or metabolite concentrations from MR spectroscopy	Concentrations of metabolites	MR	Clinical applications, clinical trials, multicentre studies, preclinical studies, ongoing validation and qualification [119, 126]

IAUGC initial area under the gadolinium concentration time curve, *BF* regional blood flow, *BV* regional blood volume, *MTT* mean transit time, *PS* permeability surface area product, *FE* blood flow extraction

also use in-house software for definition of regions of interest (ROIs) and calculation of ADCs.

Validation, qualification and clinical applications Repeatability studies have shown within-patient coefficients of variation (wCV) between 4 % and 15 % [7–9]. Multicentre studies of healthy volunteers have shown significant differences in ADC estimates between scanners from different manufacturers in some abdominal organs [10] and in grey matter and white matter [11].

ADC has been shown to be negatively correlated with histological measures of cell density in glioma [12] and in colorectal liver metastases [7]. A negative correlation has also been shown between ADC and the proportion of collagenous fibres in pancreatic cancer [13]. A study of 32 patients with locally advanced gastrooesophageal cancers showed a correlation between the change in ADC estimates after neaoadjuvant treatment and the tumour regression grade determined from histology [14]. Although an increase in ADC estimates between pretreatment and posttreatment measurements has been shown to be predictive of response to treatment in many cases, some studies have not demonstrated correlation between change in ADC and response [5].

The use of DW MRI as a biomarker has revolutionized oncological diagnosis. As it can be used both qualitatively by viewing the high b-value images and ADC maps as well as quantitatively to generate mean or median tumour ADCs, it has been exploited as a diagnostic tool, and as a prognostic/predictive biomarker as well as for longitudinally monitoring treatment response. In several tumour types, e.g. liver [15, 16], lung [17], kidney [18], breast [19], prostate [20] and cervix [21], it is used to differentiate tumour from nontumour tissue (Fig. 1). However, its quantitative potential has been exploited to predict the aggressiveness of disease in prostate cancer [22] and histological grade in renal cancer [23] and cervix cancer [24]. Change in ADC has been shown to be predictive of therapeutic response in cervix cancer [25], colorectal liver metastases [26] and ovarian cancer [8] (Fig. 2) as well as for predicting local recurrence in rectal cancer [27], endometrial cancer [28] and biochemical recurrence in prostate cancer [29]. More recently, whole-body DW MRI has become possible through advances in RF and gradient coil technology as well as software for integrating image stacks into a visual representation of the whole body in a 3D multiplanar reformat. This type of image has been used for metastases screening, particularly in patients in whom bone lesions may be the only site of disease and bone scintigraphy is negative, e.g. multiple myeloma [30]. In this whole-body mode it has the advantage of being able to estimate the total tumour burden for skeletal metastases (Fig. 3) and follow their response to treatment, which has hitherto not been possible [31].

Current limitations and future perspectives A major limitation in the validation and qualification of ADC as a biomarker in oncology is the lack of standardization for data acquisition and analysis. There are currently no standard sequences which can be implemented on all platforms which limits the extent to which data acquisition can be standardized in multicentre projects [6, 32]. Technical limitations, for example non-uniformity in ADC estimates, may introduce errors, particularly when employing large fields of view [32]. Software and methods for analysis are not standardized, leading to variation in definition of ROIs and calculation of ADCs [33].

The physiological basis of the diffusion-weighted signal is not fully understood and validation, for example by correlation with histopathology, remains an area of current and future work. The temporal evolution of ADC in response to treatment may be influenced by factors such as cell swelling, cell shrinkage, necrosis, fat infiltration and fibrosis [2, 4]. Moreover, attempts to use pretreatment ADC estimates as a predictive biomarker have yielded mixed results with some studies showing a correlation between pretreatment ADC and response to treatment while many other studies have shown no correlation [5]. A limitation of many studies is that numbers of patients have been small and meta-analyses have been impeded by differences between imaging protocols, patient populations and treatment regimens [5].

Current work is focused on qualification of ADC as a biomarker in oncology drug development [4, 34]. Work includes optimization and standardization of data acquisition, assessment of ADC as a prognostic or diagnostic biomarker in multicentre studies and histopathological validation [4, 6].

Magnetization transfer ratio

Mechanisms of contrast Magnetization transfer (MT) contrast in MRI arises from interactions between protons (hydrogen nuclei) in a bound pool, for example protons attached to macromolecules or in hydration layers, and protons in a free pool, for example mobile water protons [35]. Bound pool protons do not contribute directly to the measured signal in most conventional MR imaging (which measures freely mobile protons) owing to their short T_2 relaxation times (<1 ms) [36, 37]. The presence of protons in the bound pool may be detected via their interactions with the free pool by selectively saturating the broad resonance of the bound protons using an off-resonance RF pulse. This transfers saturation to the free pool by exchange of spins between the bound and free pools, either by chemical exchange or by dipolar coupling, and reduces the longitudinal magnetization available for imaging. This results in a reduction in signal intensity, compared to that observed without the off-resonance saturation pulse. Magnetization transfer ratio (MTR), which is the difference between the signal

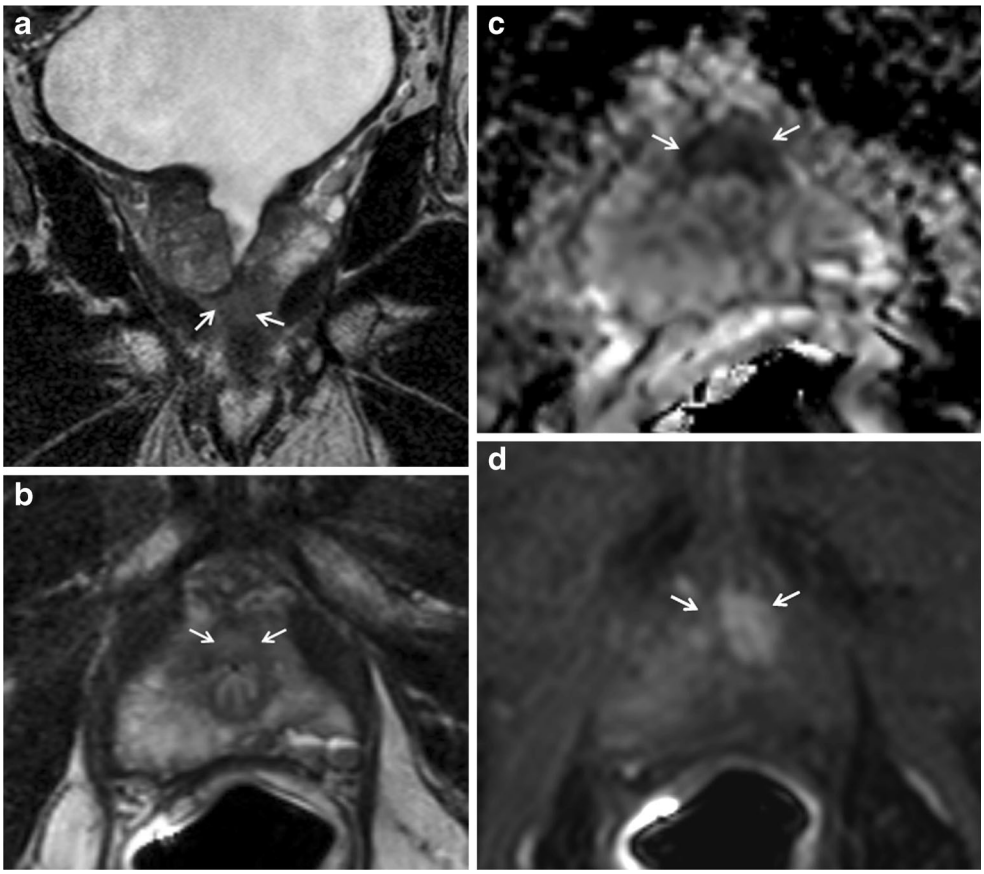

Fig. 1 Prostate cancer in an 82-year-old man. **a** Coronal and **b** transverse T_2-weighted images through the prostate apex with **c** corresponding transverse ADC map and **d** enhanced image 60 s after gadolinium administration show an anterior prostate tumour (*arrows*). The tumour is difficult to appreciate in **a** and **b**, but easily identified in **c** and **d**. The spatial mismatch between the regions of restricted diffusion in **c** and contrast enhancement in **d** is attributed to heterogeneity of the biological mechanisms determining these features within the tumour

intensity observed without the off-resonance saturation pulse (M_0) and the signal intensity observed after the saturation pulse (M_{SAT}), normalized to M_0, is used to quantify the MT effect (Eq. 2).

$$MTR = \frac{M_0 - M_{SAT}}{M_0} \quad (2)$$

Technical requirements MT sequences are available on most modern MR scanners and do not require additional hardware or software. MTR maps may be produced using manufacturers' software. As with any subtraction technique, MTR measurements are sensitive to motion and techniques such as breath-holding or cardiac gating may be required. Safety considerations, which require the specific absorption rate to be kept within regulatory limits, restrict the flip angle of the saturation pulse. Agar and albumin have been used to provide stable and reproducible MT phantoms for protocol development [37, 38].

Validation, qualification and clinical applications Unlike DW MRI, there has been no attempt at standardization of MTR for use as a biomarker in oncology. However, validation against histopathology has been reported both in preclinical studies and in neurological applications in the clinic. MTR has been correlated with histological measures of fibrosis in pancreatic tumour models [39] and with collagen content in meningiomas [40] and with volume fraction of tumour cell nuclei in astrocytomas [41] in clinical studies. One multicentre study of the brains of healthy volunteers showed significant variation in MTR histogram metrics, which the authors suggested may have been due to the difference in flip angle of the off-resonance RF pulses between scanners [42].

Current limitations and future perspectives MTR is still in the early stages of validation and qualification. MTR depends on pulse sequence and magnetic field strength [36, 37, 48] and the lack of standardization of MT sequences between scanners may contribute to differences in measurements of MT properties [42]. Development of MTR as a biomarker therefore also requires assessment of variability between scanners and standardization of sequences.

Although many studies have demonstrated the use of MTR in discriminating between benign and malignant lesions and among grades of tumours, further investigation of MTR is required in assessment of response to treatment. More advanced modelling may be used to extract other parameters to prove its utility as a response biomarker [35].

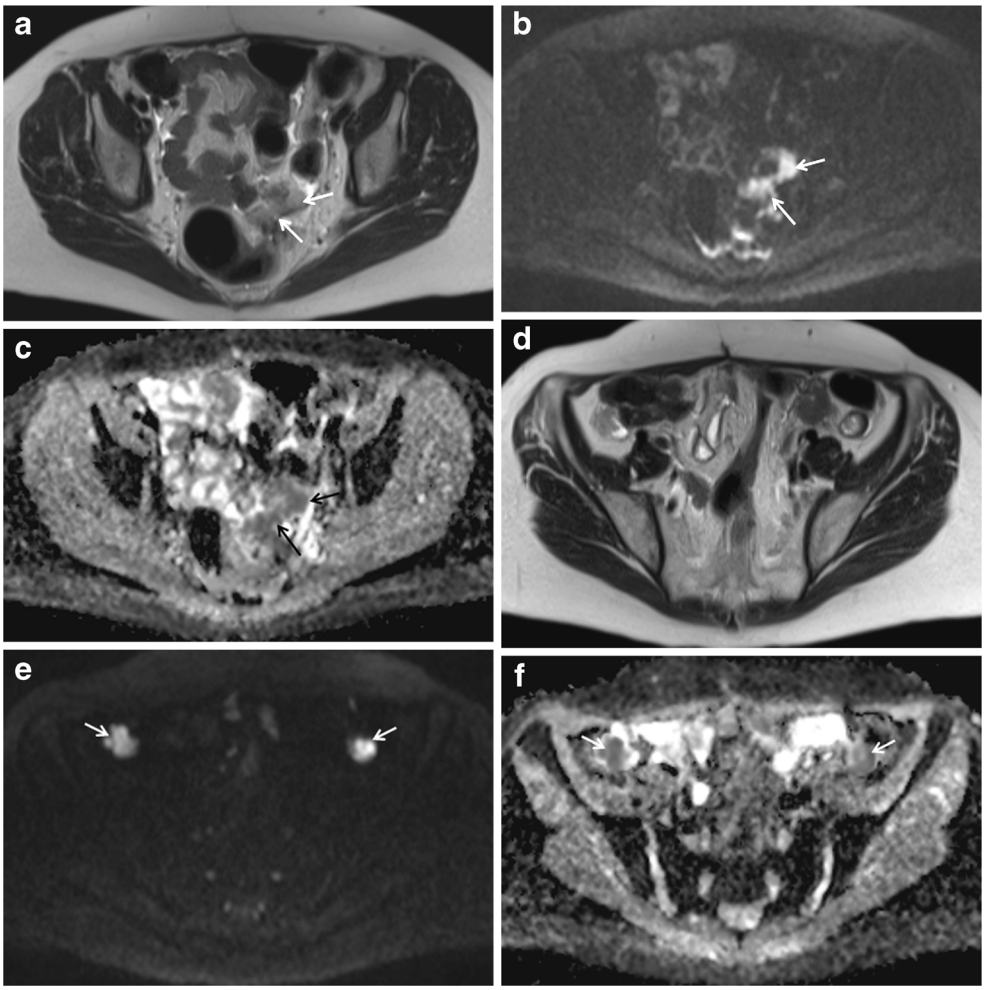

Fig. 2 Ovarian cancer in a 70-year-old woman. **a** Transverse T_2-weighted, **b** diffusion-weighted (b=1,050 s/mm^2) and **c** ADC map through the lower pelvis show irregular soft tissue with marked diffusion restriction on the right peritoneal reflection and serosal surface of the sigmoid colon (*arrows*). At a higher level in the mid pelvis **d** transverse T_2-weighted, **e** diffusion-weighted (b=1,050 s/mm^2) and **f** ADC map show bilateral peritoneal deposits (*arrows*). These are best seen in **e** and are quantifiable from **f**, but are less conspicuous in **d**

In clinical trials, two studies of brain tumours have shown higher MTR in high-grade astrocytomas than in low-grade astrocytomas [40] and in high-grade gliomas than in low-grade gliomas [41]. However, another study has shown that while tumours, infection and infarction all have significantly lower MTR than normal grey matter and white matter, the difference between MTR of high-grade and low-grade gliomas is not significant [43]. Clinical studies outside the brain include breast lesions where MTR has been used to discriminate between benign and malignant histologies [44], parotid glands [45] and prostate (Fig. 4). A feasibility study of MT imaging in patients with non-small-cell lung cancer has shown similar structures in MTR maps and FDG PET images and showed lower MTR in areas of suspected atelectasis than in tumours [46].

MTR has also been used in the detection of postradiation fibrosis. A study of patients with rectal cancer treated with neoadjuvant chemoradiotherapy showed that the mean MTR of regions of fibrosis is significantly higher than the MTR of residual tumour, normal rectal wall or oedematous rectal wall; comparison with histopathological analysis showed that MTR diagnosed fibrosis with a sensitivity of 88 % and specificity of 90 % [47].

Native T_1 relaxation time

Mechanisms of contrast T_1 relaxation time is a time constant for the recovery of longitudinal magnetization following excitation. T_1 depends on the molecular environment of water molecules as well as on magnetic field strength [49]. *Native* T_1 refers to the longitudinal relaxation time of protons in the absence of exogenous contrast agents. Changes in native T_1 may be indicative of alterations in oedema [50] or release of paramagnetic ions and proteins during the destruction of cells and tissues [51].

Technical requirements Inversion recovery and saturation recovery methods can be used to estimate T_1 but acquisition times are relatively long [52]. Spoiled gradient-echo sequences with two or more flip angles are often used when faster acquisitions are required [53]. Optimization of flip angles is required for the range of T_1 values to be measured [54].

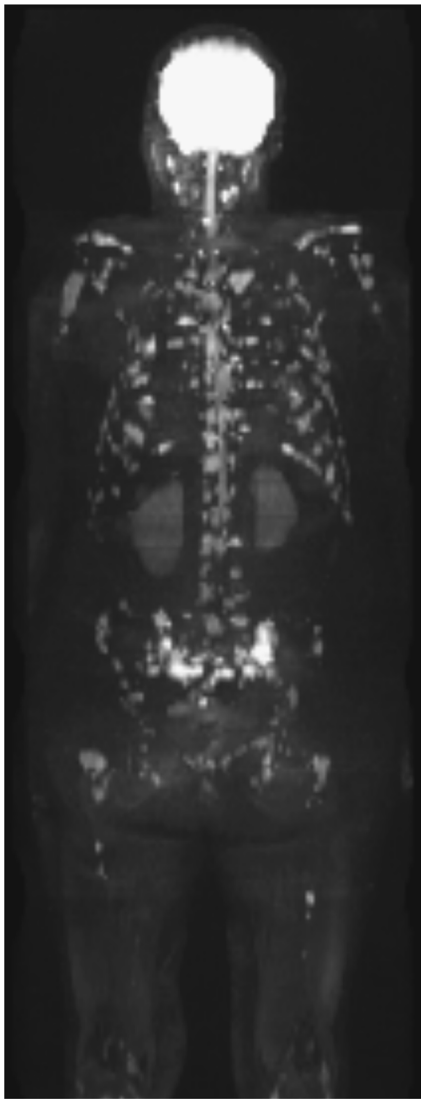

Fig. 3 Whole-body diffusion-weighted image in a 67-year-old woman with biopsy-proven multiple myeloma. The coronal plane is reconstructed from data acquisition in the transverse plane in multiple stacked volumes and displayed as an inverted grey scale of the b= 1,050 s/mm^2 images. Focal areas of restricted diffusion are noted throughout the skeleton indicative of focal sites of myelomatous deposits within bone marrow

Inhomogeneities in transmit B_1 field can cause errors in T_1 estimates values due to errors in flip angles [55].

Validation, qualification and clinical applications Native T_1 of tumours has been shown to correlate with decreases in tumour volume in a TH-MYCN transgenic mouse model of neuroblastoma treated with cyclophosphamide, a vascular disrupting agent (ZD6126) or an antiangiogenic agent (cediranib) [56]. Similar correlations have been observed in two mouse tumour models treated with an mTOR inhibitor (everolimus) [51] and in eight tumour models treated with five different chemotherapeutic agents where 15 – 20 % reductions in native T_1 were seen in all cases of successful chemotherapy compared to controls, but not in drug-resistant models [57]. However, this needs to be considered in the context of reproducibility: a study of patients with metastatic colorectal cancer found a wCV of 15.8 % for baseline T_1 measurements [58].

Only a small number of published studies have assessed native T_1 as a biomarker in the clinic [50]. In a pilot study of ten patients with metastatic colorectal cancer a reduction in native T_1 was seen in tumours treated with an anti-VEGF monoclonal antibody (bevacizumab) compared to pretreatment values [58]. Another study of 27 patients with acute leukaemia showed longer native T_1 of vertebral bone marrow measured at diagnosis, compared with age-matched controls, and showed a decrease in T_1 with treatment in patients who went on to obtain remission but persistently long T_1 in patients who did not achieve remission [59].

Current limitations and future perspectives The measurement of native T_1 in multicentre trials is limited because good B_0 and B_1 homogeneity may be difficult to achieve, particularly over large fields of view or at higher field strengths. There is not yet a standard method of acquisition or analysis of data for estimation of native T_1 as a biomarker in oncology. Future studies are required to investigate treatment-induced changes in T_1, assess reproducibility of T_1 measurements and validate observations against histological analysis. Accuracy, precision and reproducibility of T_1 measurements can be assessed using phantoms containing materials of appropriate size, location and T_1 [55].

Vascular biomarkers

Dynamic contrast-enhanced MRI

Mechanisms of contrast DCE MRI provides information about the structure and function of the microvasculature [50, 55]. The term DCE MRI is used to refer to T_1-weighted DCE imaging, whereas the term dynamic susceptibility-contrast (DSC MRI) is used to refer to T_2*-weighted or T_2-weighted DCE imaging [60]. DCE MRI uses a bolus injection of a paramagnetic gadolinium-based contrast agent to reduce the T_1 of nearby protons and increase the signal intensity on a T_1-weighted image. Estimation of T_1 at each spatial and temporal position, combined with estimates of T_1 before injection and knowledge of the relaxivity of the contrast agent, allows estimation of the concentration of gadolinium in each voxel over time [55]. Analysis of the gadolinium concentration–time curve using pharmacokinetic models or model-free approaches allows estimation of parameters related to the delivery of contrast agent to the tumour volume, the surface area and permeability of capillaries, the volume of the extracellular extravascular space (EES) and the blood plasma volume [55].

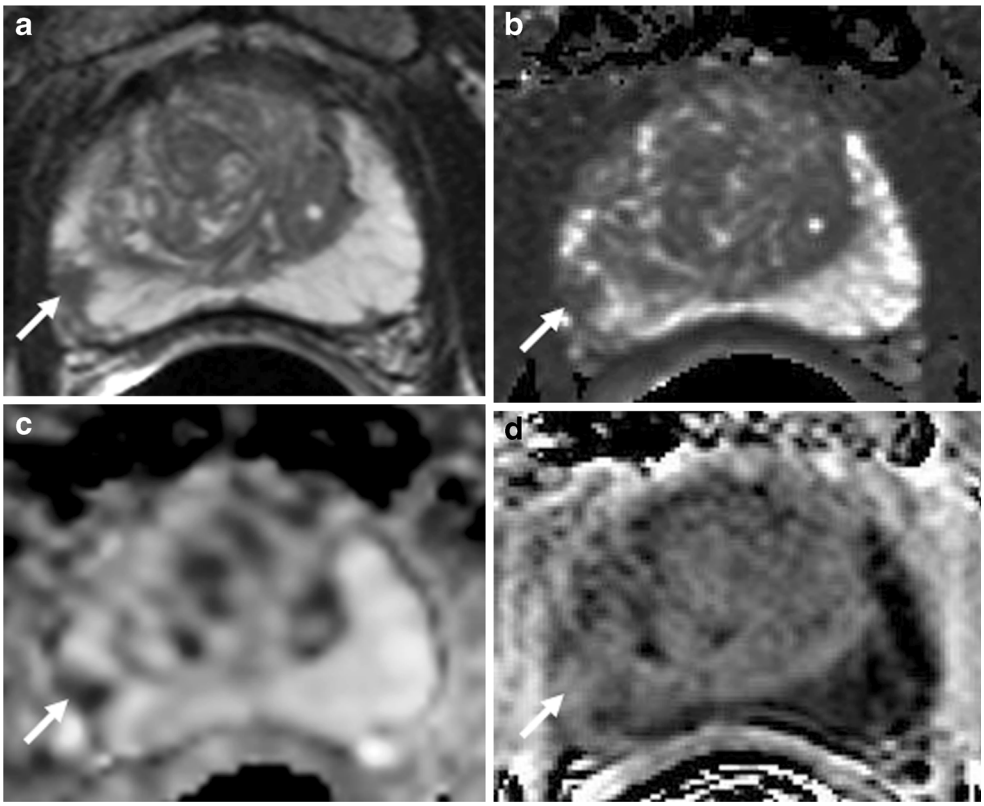

Fig. 4 Prostate cancer in a 63-year-old man. **a** Transverse T_2-weighted image through the mid-prostate shows a low signal intensity tumour in the right peripheral zone (*arrow*). **b** Corresponding T_2 map, **c** ADC map (calculated from data acquired at b=0 s/mm^2 and 800 s/mm^2) and **d** magnetization transfer contrast image (subtraction of data acquired without and with a 1,000 Hz off-resonance pulse) show a short T_2 lesion (**b**, *arrow*) with restricted diffusion (**c**, *arrow*) and very little magnetization transfer effect (**d**, *arrow*) compared to the peripheral zone on the left

Technical requirements DCE MRI requires rapid T_1-weighted imaging before injection of a contrast agent, during injection and for several minutes (>5 min) after injection. Three-dimensional spoiled gradient-echo sequences are usually employed to achieve good temporal resolution (approximately 5 – 20 s) [55, 61, 62]. T_1 can be estimated from two gradient-echo images acquired with different flip angles [53]. The larger flip angle is often acquired after injection of the contrast agent and combined with a low-flip-angle precontrast image to allow more rapid imaging. A power injector is usually used to provide reproducible administration of the contrast agent [55].

Pharmacokinetic models are often used to analyse the gadolinium concentration–time curve [60, 63, 64]. Off-line analysis is required using commercial or in-house software. Published recommendations state that the Tofts model, or equivalent, should be used and that the initial area under the gadolinium concentration–time curve (IAUGC) and the volume transfer constant (K^{trans}) should be reported as primary end-points [55]. Other parameters, for example volume of EES per unit volume of tissue (v_e) and blood plasma volume per unit volume of tissue (v_p), are also reported in some studies, as well as model-free parameters, for example enhancing fraction [50].

Pharmacokinetic models require estimation of the arterial input function (AIF) which may be directly estimated from the DCE MRI data using an artery present in the images, or estimated using an additional sequence before the main DCE sequence using a prebolus of gadolinium; population-based estimates of AIF have also been applied [55].

Validation, qualification and clinical applications Consensus recommendations have been published for the use of DCE MRI in early-stage clinical trials of antivascular and antiangiogenic therapies [55]. Recommendations for standardization of nomenclature in DCE MRI models have been produced [64]. Repeated baseline measurements in clinical studies have estimated the wCV of K^{trans} and IAUGC to be around 15 – 20 %. [65, 66]. On comparison with histology, correlations between DCE MRI parameters and microvessel density have been demonstrated [62].

Changes in DCE MRI parameters with treatment, for example reduction in K^{trans} but also other changes, have been reported in a variety of tumours (Figs. 1 and 5) and summarized in several reviews [50, 61, 62, 67]. A large number of these trials have been in a phase I setting with novel antiangiogenic agents [68–70] and have been particularly useful in paediatrics where radiation dose is a consideration [71]. In addition to its role in monitoring treatment response, there is an extensive literature on the utility of DCE MRI to predict patient outcomes [72–74]; for example, enhancement patterns predict overall survival (OS) in women with breast cancer undergoing neoadjuvant chemotherapy [75] and in patients with renal cell cancer [76].

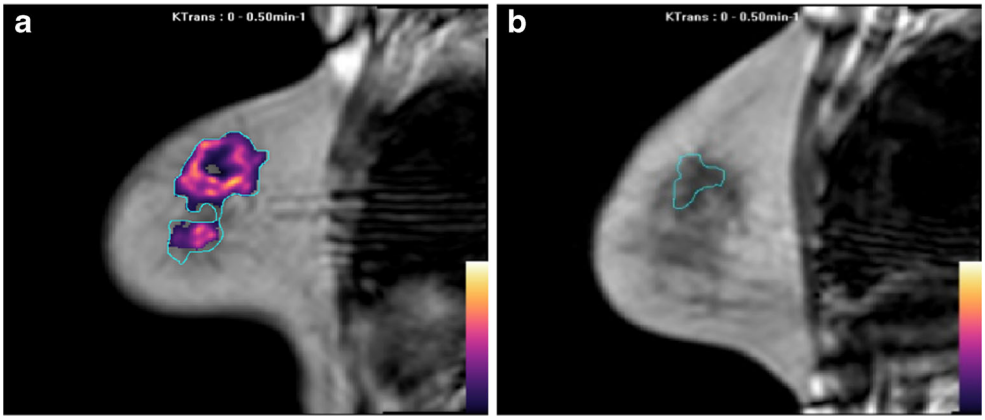

Fig. 5 K^{trans} map of a large locally invasive breast cancer demonstrating radiological response. **a** Pretreatment image. **b** Posttreatment image shows a reduction in enhancement after two cycles of epirubicin and cyclophosphamide

Current limitations and future perspectives Implementation in multicentre trials is challenging as there are no standardized protocols for DCE MRI data acquisition [50, 55]. Analysis is done off-line and a range of models and software packages are available. Parameters derived from pharmacokinetic models depend on the choice of AIF [50, 55, 67]. The choice of ROIs also affects the results, and the methods for defining these are not standardized [55, 67]. Appropriate strategies for assessing heterogeneity and motion are also topics of current research [61].

Modelled parameters are dependent on many physiological processes, and interpretation is not straightforward [61]. The optimal timing of examinations relative to treatment is also unknown and DCE MRI may fail to detect an effect if there are rapid changes followed by a return to baseline properties after treatment [50]. Repeatability of DCE MRI parameters has been reported to be 15 – 20 %, which limits the size of change that can be detected. Changes in DCE MRI parameters found in phase I/II trials have not always translated into significant differences in progression-free survival or OS in phase III trials [67]. Going forward, standardization of acquisition and analysis methodology is crucial to successfully incorporate this biomarker as a robust imaging read-out in multicentre response assessment trials [34, 50].

Dynamic contrast-enhanced CT

Mechanisms of contrast DCE CT provides information about tumour vasculature using rapid imaging before, during and after injection of an iodinated contrast agent. Pharmacokinetic modelling is used to estimate physiologically based parameters, for example blood flow per unit volume or mass of tissue (regional blood flow, BF), fraction of tissue that consists of flowing blood (regional blood volume, BV), time for the contrast agent to traverse the vasculature (mean transit time), rate of transfer of contrast agent from intravascular to extravascular space (blood flow extraction product, FE product) and permeability and surface area of capillary endothelium (permeability surface area product; Fig. 6) [77].

Technical requirements Consensus guidelines recommend multislice imaging with high temporal resolution (about 2 s) [77]. Processing software is provided by the equipment manufacturers and is straightforward to acquire and robust to model because of the linear relationship between contrast agent uptake and increase in tissue density.

Validation, qualification and clinical applications Consensus guidelines have been published for the use of DCE CT in oncology [77]. Repeatability studies have estimated wCV 16 % and 30 % for DCE CT parameters in preclinical [78] and clinical studies [66], respectively, which are similar to those for DCE MRI parameters. A multicentre study using a flow phantom showed minimal differences between DCE CT parameters among three institutions using a standardized protocol, which is a significant advantage for multicentre trials, but emphasizes that tube current and reconstruction methods could significantly affect results [79].

DCE CT vascular parameters have been shown to correlate with histological assessments of hypoxia [80] as well as with microvessel density [81]. DCE CT therefore has been used extensively in clinical trials where changes in BF, BV, FE product, and other parameters, have been used to demonstrate effects of various drugs in a variety of tumour sites [77, 82]. Key studies have been performed in non-small-cell lung cancer treated with sorefanib and erlotinib [83] or with radiotherapy [84], and in nasopharyngeal carcinoma treated with pazopanib [85] and cediranib in a phase I setting [66].

Current limitations and future perspectives Radiation dose may be significant and should be kept as low as reasonably achievable whilst maintaining acceptable image quality [77]. This is a significant limitation in longitudinal studies. As with DCE MRI, software for analysis has not been standardized and there may be variation among results obtained from postprocessing software from different manufacturers [79, 86]. As with MRI, inclusion of DCE CT in multicentre studies requires standardization of acquisition protocols, QA procedures and analysis software [86].

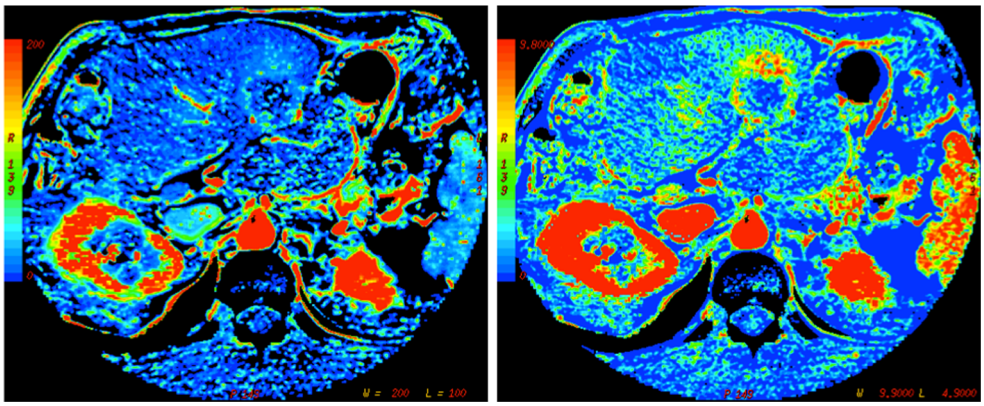

Fig. 6 Maps of **a** blood flow and **b** blood volume calculated from DCE CT

Transverse relaxation rate

Mechanisms of contrast Transverse relaxation rate (R_2*), which is the reciprocal of the transverse relaxation time (R_2*=1/T_2*), describes the rate of dephasing of transverse magnetization following excitation. R_2* is determined by spin–spin interactions, inhomogeneities in the applied magnetic field (B_0) and magnetic susceptibility variations in the tissue. In tumours R_2* may reflect the presence of paramagnetic species, such as deoxyhaemoglobin, and may be related to oxygenation levels. It has also been suggested that a decrease in R_2* in response to carbogen inhalation may reflect increased oxygenation in tumours which are hypoxic but have a functional vasculature [87–89]. An example R_2* map is shown in Fig. 7.

Technical requirements R_2* can be estimated using a multiecho gradient-echo sequence. A log-linear plot of signal intensity against echo time has a gradient of $-R_2$*. Good SNR, shimming and minimal motion between images are required.

Validation, qualification and clinical applications Pre clinical studies have shown that baseline R_2* and carbogen-induced changes in R_2* estimates are correlated with histological assessments of hypoxia [88] and with tumour pO_2 measured using a fibre-optic oxygen sensor [89]. A study carried out in a Th-MYCN genetically engineered mouse model of neuroblastoma showed slower baseline R_2*, smaller change in R_2* in response to 100 % oxygen and lower uptake of the perfusion marker Hoechst 33342 in tumours harbouring the ALK^{F1174L} mutation, known to be associated with poorer prognosis in children with neuroblastoma, compared with tumours in the Th-MYCN cohort [90]. Pretreatment estimates of R_2* and carbogen-induced ΔR_2* have also been shown to be predictive of acute response to radiotherapy in two animal models, which the authors suggested may correspond to oxygenation levels of the tumours [91]. In assessment of response to chemotherapy, one preclinical study showed a decrease in R_2* after treatment with a vascular disrupting agent (ZD6126) [92] while a study in another model showed increased R_2* after treatment with an antiangiogenic agent (cediranib) but no change compared with controls in mice treated with either cyclophosphamide or a vascular disrupting agent (ZD6126) [56].

Only a small number of studies have demonstrated clinical applications of R_2* as a biomarker in oncology. A study in breast cancer showed lower R_2* in tumours than in normal breast tissue with an increase in R_2* in tumours after neoadjuvant chemotherapy and a larger increase in responding patients than in nonresponding patients [93]. As with preclinical models, human studies have shown conflicting data; a correlation between R_2* estimates in prostate tumours and measures of hypoxia determined by needle electrode oxygen measurements was demonstrated in one study [94] while another study in hepatocellular carcinoma showed that neither baseline R_2* estimates nor R_2* measured after inhalation of 100 % oxygen were able to detect microvascular invasion when compared to histopathological analysis [95]. As with DCE CT and

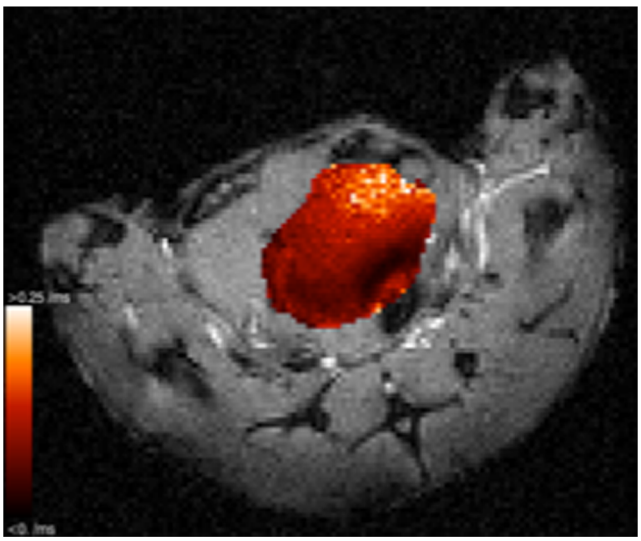

Fig. 7 R_2* map acquired from an orthotopic PC3 prostate cancer xenograft

MRI data, wCV of R_2* in pelvic tumours is 17.5 % before treatment [65].

Current limitations and future perspectives R_2* has performed poorly compared with other imaging biomarkers. Changes in R_2* between pretreatment and posttreatment measurements have performed worse than DCE MRI and DSC MRI in prediction of response to neoadjuvant chemotherapy in patients with breast adenocarcinoma [93]. It has been suggested that the increases and decreases in R_2* estimates in response to treatment result from a combination of vascular effects; haemorrhage and other pathological changes in the tumour may contribute to observed changes in R_2* and that estimates of R_2* cannot discriminate between these changes [87, 92].

Vessel size index

Mechanisms of contrast Vessel size index (VSI) is the average diameters of blood vessels within a voxel. Injection of a paramagnetic or superparamagnetic contrast agent causes different changes in R_2 and R_2*, and the ratio $\Delta R_2^*/\Delta R_2$ has been shown to be related to vessel sizes in tumours and normal tissues [96]. Analytical expressions have been derived relating VSI to $\Delta R_2^*/\Delta R_2$, the change in magnetic susceptibility of blood due to the contrast agent ($\Delta\chi$) and ADC [97, 98]. An example VSI map is shown in Fig. 8.

Technical requirements ΔR_2 and ΔR_2* can be measured using spin-echo and gradient-echo sequences, respectively. Pre clinical experiments have used steady-state experiments using ultrasmall paramagnetic iron oxide (USPIO) contrast agents, which are assumed to remain in the blood pool [96]. Estimates of $\Delta\chi$ can be obtained from ex vivo measurements [97]. ΔR_2* and ΔR_2 have also been estimated using first-pass dynamic sequences with gadolinium-based contrast agents in clinical and preclinical studies [99–101].

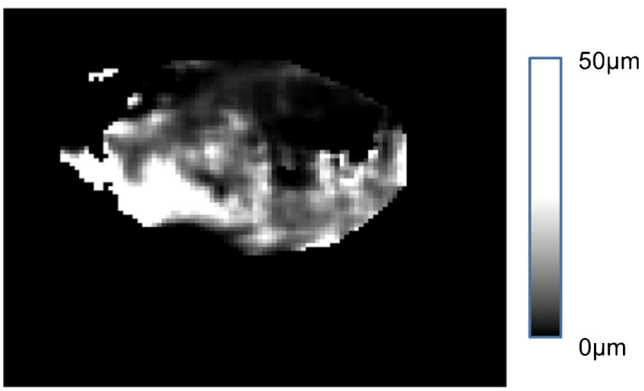

Fig. 8 VSI map acquired from a murine B16 melanoma xenograft

Validation, qualification and clinical applications Although correlation has been shown between VSI estimated from MRI and histological analysis, MRI overestimates VSI compared to histology [102], two-photon laser scanning microscopy [103], intravital microscopy [104] and micro-CT [105]. Conversely, other studies have shown good agreement between VSI estimates from in vivo MRI and ex vivo measurements of vascular casts using micro-CT [106]. Pre clinical studies have shown increases in mean VSI in tumours treated with antivascular agents, attributed to loss of small functional vessels; histological analysis have shown similar relative changes despite the discrepancy in absolute values [107, 108]. Other studies, however, have shown a decrease in VSI after treatment [109].

Only a small number of clinical studies have used VSI in a clinical trial setting. One study in gliomas showed a correlation between $\Delta R_2^*/\Delta R_2$ and tumour grade [99] whilst another study of 16 patients with glioblastoma used maps of relative tumour vessel size to show reduction in tumour vessel size in patients treated with a pan-VEGF receptor tyrosine kinase inhibitor as part of a phase II trial [100].

Current limitations and future perspectives Early development of USPIOs for clinical use was halted but the use of ferumoxytol has recently been reported in DSC MRI [110]. Motion may also affect estimates of VSI, particularly in extracranial applications. Overestimation of VSI, due to simplifying assumptions in the model [98] or inability to detect vessels that are not perfused by the contrast agent [102], may limit VSI to relative rather than absolute measurements. Therefore, although relative changes in VSI have shown promise in preclinical measurements, validation of quantitative results is required.

Relative blood volume

Mechanisms of contrast Relative blood volume (rBV) is the proportion of a voxel that is composed of blood. Injection of a paramagnetic or superparamagnetic contrast agent causes a change in R_2* which is dependent on the vascular architecture. Analytical expressions have been derived relating rBV to ΔR_2^* and $\Delta\chi$ [97]. An example rBV map is shown in Fig. 9.

Technical requirements R_2* can be measured using gradient-echo sequences. In pre clinical experiments involving steady-state experiments USPIO contrast agents have been used which can be assumed to remain in the blood pool [97]. In clinical studies DSC MRI has been used with injection of gadolinium-chelate contrast agents or, more recently, the USPIO ferumoxytol [110].

Validation, qualification and clinical applications Reductions in rBV have been shown in preclinical studies of tumours

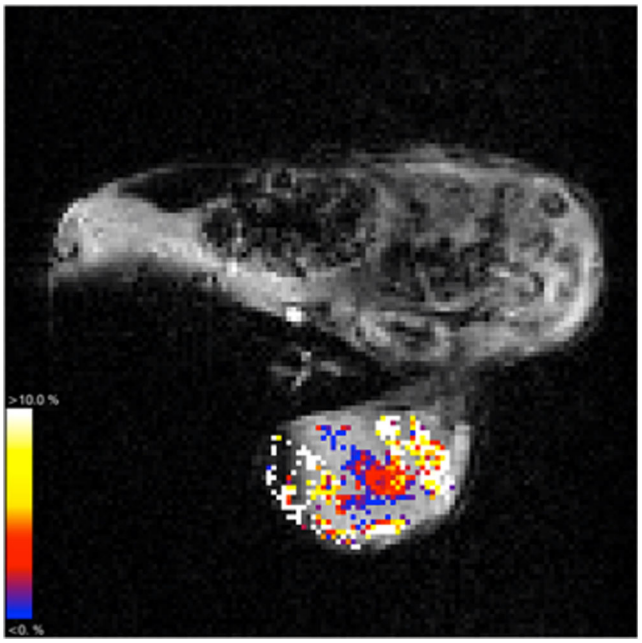

Fig. 9 rBV map acquired from a 786-O RCC xenograft using susceptibility-contrast MRI with USPIO particles

treated with antiangiogenic [107] and vascular disrupting agents [109] in good agreement with histology results, which have shown reduction in perfusion in the treated tumours. In vivo MRI has been shown to overestimate rBV compared with ex vivo micro-CT [105] or two-photon laser scanning microscopy [103]. Some preclinical studies have shown good agreement between estimates of rBV from MRI and histological measurements of blood volume [111] although other studies have shown that estimates of rBV from MRI are larger than estimates from histology [102].

In clinical studies, wCV of rBV in pelvic tumours was 19.7 %, similar to DCE MRI parameters [65]. rBV has been shown to be able to distinguish between types and grades of brain tumours [112] and to distinguish recurrence or progression from posttreatment radiation effects, necrosis and pseudoprogression [110, 113]. rBV has also been shown to be predictive of time to progression or OS in gliomas [114]. A small number of studies of rBV have been carried out in extracranial tumours [115]. One pilot study in ten patients with renal cell carcinoma showed a decrease in rBV after treatment with sunitinib [116]. A study in 37 patients with breast cancer treated with neoadjuvant chemotherapy showed that the change in rBV between pretreatment and posttreatment scans was correlated with clinical and pathological response [117]. A study of 20 patients with prostate cancer showed a decrease in rBV 1 month after starting androgen deprivation therapy [118].

Current limitations and future perspectives Although rBV has been used in many clinical studies for the assessment of brain tumours, only a small number of studies have investigated extracranial tumours. As with other vascular biomarkers, standardized methods for acquisition or analysis of rBV estimates from DSC MRI or steady-state measurements are lacking, which precludes implementation of this biomarker in a multicentre setting. As applications in brain tumours have far exceeded extracranial applications for this biomarker, attempts at standardization in brain protocols is currently underway. Further biological validation, however, is urgently needed [115].

Metabolic biomarkers

Magnetic resonance spectroscopy Magnetic resonance spectroscopy (MRS) uses largely the same hardware as MRI, but instead of acquiring high-resolution images of water and lipid distribution and their properties, it acquires signals from compounds of low molecular weight in tissue that have concentrations of a few millimoles. MRS can therefore probe biochemistry and metabolism in tissue. In addition to tissue characterization, it can also be used to help evaluate response and recurrence, and aid treatment planning. Example ^{1}H MR spectra are shown in Fig. 10.

Technical requirements Signals are acquired either from a single specified voxel or from a 2D or 3D array of voxels using some form of MRS imaging. The minimum useful voxel size depends on magnetic field strength, RF coil design, scan duration and the question being addressed, and is typically about 10 – 20 mm. Methods are well-described in the literature [119]. Manufacturers provide some software for spectral data processing, display and fitting, but many users will also process data off-line using specialized spectral processing packages such LCModel [120, 121] and jMRUI [122–124]. Results are commonly expressed as ratios of peak areas within the spectrum, or relative to signal from tissue water (for ^{1}H MRS). Calculation of metabolite concentrations is possible if values for the T_1 and T_2 relaxation time constants of the metabolites are known, and where the RF transmit and receive fields are either uniform or amenable to calculation. To acquire MRS signals from magnetic nuclei other than ^{1}H requires a RF system (coils, amplifiers, detectors etc.) that operate at the appropriate MR frequency.

Proton MRS and its clinical applications Most MRS studies use signals acquired from ^{1}H nuclei of compounds in tissue, since ^{1}H nuclei provide the largest signals, and this requires no hardware modification to the scanner. ^{1}H MR spectra of normal brain are dominated by choline, creatine, and N-acetyl aspartate (Fig. 10). Brain tumours are characterized by reduced N-acetyl aspartate, and often by elevated total choline

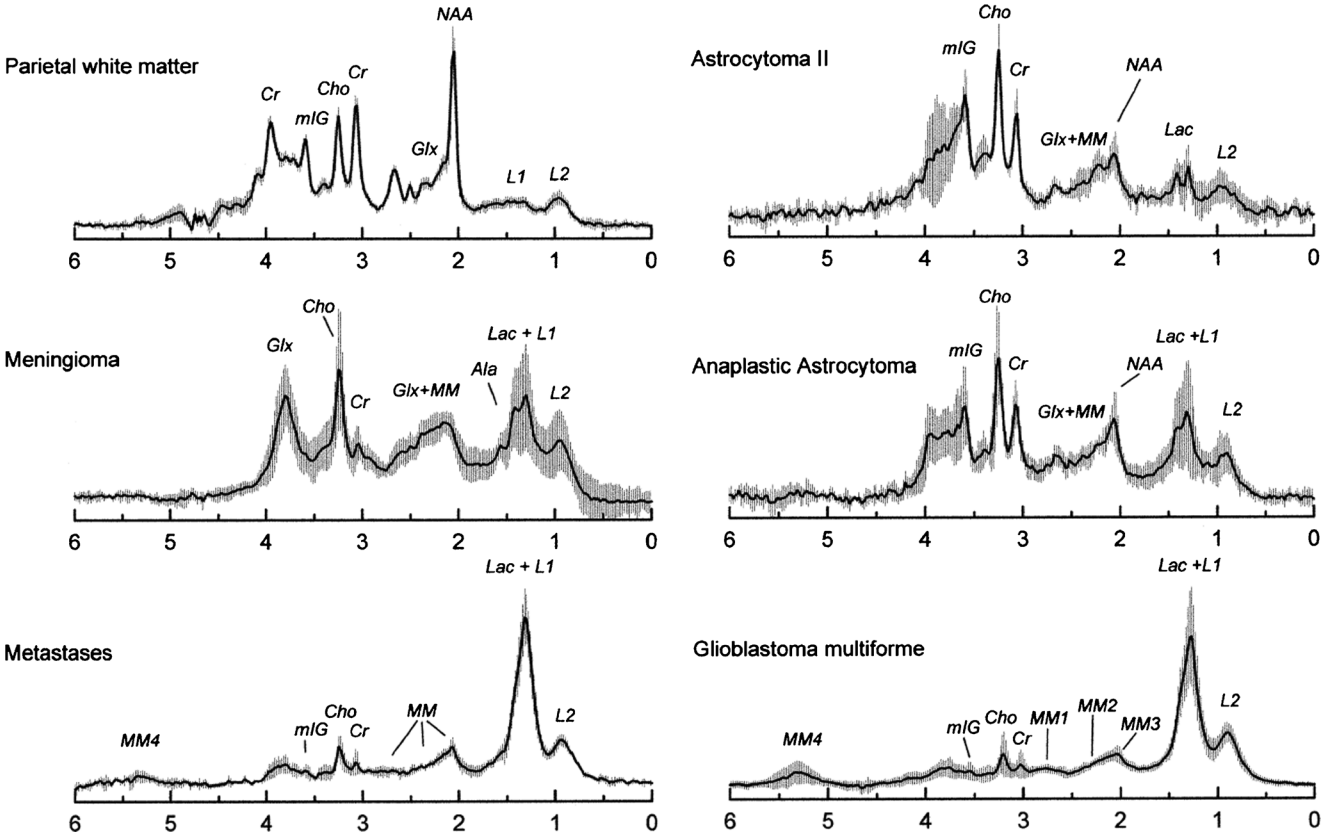

Fig. 10 Means and standard deviations (*vertical lines*) of normalized STEAM (echo time 30 ms) spectra: normal (parietal) white matter (N=6), meningioma (N=8), metastases (N=6), astrocytoma grade II (N=5), anaplastic astrocytoma (N=7), glioblastoma (N=13). Reproduced from Howe et al. [126]

(which includes choline, phosphocholine and glycerophosphocholine), lipid or lactate. Elevated choline is attributed to increased proliferation and demand for membrane synthesis, while lactate may be caused by a combination of increased lactate production owing to the Warburg effect [125] together with inadequate perfusion to remove it. Different brain tumours have different metabolic fingerprints, yielding the possibility of using ^{1}H MRS for differential diagnosis [126] (Fig. 10). Regions of metabolic abnormality sometimes extend beyond regions of imaging abnormality [127], demonstrating that MRS can detect regions of tumour not detected by standard MRI.

Elevated choline is characteristic of tumours in other tissues also, such as breast [128] and prostate [129]. Prostate tumours also have reduced citrate and spermine [129]. Some tumours exhibit high levels of lipids, in particular high-grade glioma and metastases in the brain [126]. These signals arise from cytoplasmic lipid droplets rather than from the membranes of cells and organelles, as lipids in bilayers are relatively immobile and produce signals that are too broad to be detected using standard MRS methods. They are associated with proliferation, inflammation, malignancy, necrosis and apoptosis [130, 131]. In tissues such as breast and prostate care is required to ensure that signals acquired are not contaminated by those of surrounding lipid.

Nonproton MRS and its clinical applications ^{31}P MRS gives lower signals than ^{1}H MRS but is useful for probing energy metabolism (phosphocreatine, ATP, NADH) and some compounds involved in membrane synthesis and breakdown, in particular phosphomonoesters (PME) such as phosphoryl choline, and phosphodiesters (PDE) such as glycerophosphorylcholine. Cancers tend to be characterized by elevated PME and PDE, but relatively normal ATP. Many studies have demonstrated a reduction in PME in response to treatment [132, 133]. In non-Hodgkin's lymphoma a multicentre trial has also demonstrated that ^{31}P MR spectra acquired before treatment contain prognostic information; tumours with an initially lower PME/NTP ratio are more likely to respond than those with a high PME/NTP [134]. ^{31}P MRS can also be used to measure intracellular pH [135, 136]. Applying this method to tumours has yielded the surprising result that tumours generally tend to maintain a slightly alkaline intracellular pH in spite of the Warburg effect [137]. Measurement of intracellular pH in vivo would be useful in assessing the effects of anticancer strategies that are

anticipated to alter pH, such as inhibitors of monocarboxylate transporters [138].

^{19}F MRS yields signals almost as strong as ^{1}H MRS. While there is little MR-visible ^{19}F in the body, ^{19}F MRS has been used to follow the distribution and metabolism of anticancer drugs such as 5-fluorouracil [139] and to study hypoxia using perfluorocarbons [140] and fluorinated nitroimidazoles [141].

Current limitations and future perspectives Magnetic resonance spectroscopy has great potential for probing metabolism and biochemistry of tissues in vivo, but is often limited by the relatively low SNR. Dynamic nuclear polarization is a new method in which atomic nuclei of compounds with large longitudinal relaxation time constants can be prepolarized to yield signals 10,000-fold larger than the normal polarization. The first-in-human trial of this method has recently demonstrated potential for imaging highly elevated pyruvate-to-lactate conversion in prostate tumours [142]. However, the full potential of this technique in providing information on metabolic pathways and thus monitoring enzyme kinetics remains to be exploited.

Conclusion

A range of biomarkers providing information on tissue organization, vascular properties and metabolism are available with MRI supported by vascular biomarkers with CT. Their potential for delivering information not only for response assessment, which has traditionally been the case, but also to predict disease aggressiveness, treatment response and outcomes of therapy offers rich avenues for exploration. Even in response assessment, it is expected that these biomarkers will deliver information on how the tumour is responding much earlier than has hitherto been possible, thus sparing the patient the morbidity of ineffective therapy and the opportunity to switch to a more effective treatment regimen earlier. As we uncover information on the heterogeneity of these biomarkers, it will also become clear which biomarker combinations are most informative, as it is unlikely that a single parameter will contain the depth of information required. Finally, in order to exploit these biomarkers fully in large multicentre trials, it is imperative that we achieve standardization with consensus on acquisition and analysis protocols that optimizes reproducibility of the measurements and allows pooling of multisite data.

Acknowledgments We acknowledge CRUK and EPSRC Cancer Imaging Centre in association with MRC and Department of Health C1060/A10334, and NHS funding to the NIHR Biomedicine Research Centre and the Clinical Research Facility in Imaging. We also acknowledge the support of the National Institute for Health Research, through the Cancer Research Network (NCRN), and acknowledge in particular Mrs Sharon Giles, Dr Elizabeth O'Flynn, Dr Matthew Orton, Dr Christina Messiou, Dr Simon Robinson and Dr Franklyn Howe for the figures used in this article.

Conflicts of interest None.

References

1. Charles-Edwards EM, de Souza NM. Diffusion-weighted magnetic resonance imaging and its application to cancer. Cancer Imaging. 2006;6:135–43.
2. Patterson DM, Padhani AR, Collins DJ. Technology insight: water diffusion MRI – a potential new biomarker of response to cancer therapy. Nat Clin Pract Oncol. 2008;5(4):220–33.
3. LeBihan D, Turner R, Moonen CT, Pekar J. Imaging of diffusion and microcirculation with gradient sensitization: design, strategy and significance. J Magn Reson Imaging. 1991;1(1):7–28.
4. Sinkus R, Van Beers BE, Vilgrain V, de Souza N, Waterton JC. Apparent diffusion coefficient from magnetic resonance imaging as a biomarker in oncology drug development. Eur J Cancer. 2012;48:425–31.
5. Heijmen L, Verstappen MC, ter Voert EE, Punt CJ, Oyen WJ, de Geus-Oei L-F, et al. Tumour response prediction by diffusion-weighted MR imaging: ready for clinical use? Crit Rev Oncol Hematol. 2012;83:194–207.
6. Padhani AR, Lu G, Koh DM, Chenevert TL, Thoeny HC, Takahara T, et al. Diffusion-weighted magnetic resonance imaging as a cancer biomarker: consensus and recommendations. Neoplasia. 2009;11(2):102–25.
7. Heijmen L, ter Voert EE, Nagtegaal ID, Span P, Bussink J, Punt CJ, et al. Diffusion-weighted MR imaging in liver metastases of colorectal cancer: reproducibility and biological validation. Eur Radiol. 2013;23:748–56.
8. Kyriazi S, Collins DJ, Messiou C, Pennert K, Davidson RL, Giles SL, et al. Metastatic ovarian and primary peritoneal cancer: assessing chemotherapy response with diffusion-weighted MR imaging – value of histogram analysis of apparent diffusion coefficients. Radiology. 2011;261(1):182–92.
9. Koh D-M, Blackledge M, Collins DJ, Padhani AR, Wallace T, Wilton B, et al. Reproducibility and changes in the apparent diffusion coefficient of solid tumours treated with combretastatin A4 phosphate and bevacizumab in a two-centre phase I clinical trial. Eur Radiol. 2009;19:2728–38.
10. Donati OF, Chong D, Nanz D, Boss A, Froehlich JM, Andres E, et al. Diffusion-weighted MR imaging of upper abdominal organs: field strength and intervendor variability of apparent diffusion coefficients. Radiology. 2014;270(2):454–63.
11. Sasaki M, Yamada K, Watanabe Y, Matsui M, Ida M, Fujiwara S, et al. Variability in absolute apparent diffusion coefficient values across different platforms may be substantial: a multivendor, multi-institutional comparison study. Radiology. 2008;249(2):624–30.
12. Sugahara T, Korogi Y, Kochi M, Ikushima I, Shigematu Y, Hirai T, et al. Usefulness of diffusion-weighted MRI with echo-planar technique in the evaluation of cellularity in gliomas. J Magn Reson Imaging. 1999;9:53–60.
13. Muraoka N, Uematsu H, Kimura H, Imamura Y, Fujiwara Y, Murakami M, et al. Apparent diffusion coefficient in pancreatic cancer: characterization and histopathological correlations. J Magn Reson Imaging. 2008;27:1302–8.
14. De Cobelli F, Giganti F, Orsenigo E, Cellina M, Esposito A, Agostini G, et al. Apparent diffusion coefficient modifications in assessing gastro-oesophageal cancer response to neoadjuvant

treatment: comparison with tumour regression grade at histology. Eur Radiol. 2013;23:2165–74.
15. Haradome H, Grazioli L, Morone M, Gambarini S, Kwee TC, Takahara T, et al. T2-weighted and diffusion-weighted MRI for discriminating benign from malignant focal liver lesions: diagnostic abilities of single versus combined interpretations. J Magn Reson Imaging. 2012;35(6):1388–96.
16. Cieszanowski A, Anysz-Grodzicka A, Szeszkowski W, Kaczynski B, Maj E, Gornicka B, et al. Characterization of focal liver lesions using quantitative techniques: comparison of apparent diffusion coefficient values and T2 relaxation times. Eur Radiol. 2012;22(11): 2514–24.
17. Wu LM, Xu JR, Hua J, Gu HY, Chen J, Haacke EM, et al. Can diffusion-weighted imaging be used as a reliable sequence in the detection of malignant pulmonary nodules and masses? Magn Reson Imaging. 2013;31(2):235–46.
18. Razek AA, Farouk A, Mousa A, Nabil N. Role of diffusion-weighted magnetic resonance imaging in characterization of renal tumors. J Comput Assist Tomogr. 2011;35(3):332–6.
19. Ei Khouli RH, Jacobs MA, Mezban SD, Huang P, Kamel IR, Macura KJ, et al. Diffusion-weighted imaging improves the diagnostic accuracy of conventional 3.0-T breast MR imaging. Radiology. 2010;256(1):64–73.
20. Mazaheri Y, Shukla-Dave A, Hricak H, Fine SW, Zhang J, Inurrigarro G, et al. Prostate cancer: identification with combined diffusion weighted MR imaging and 3D 1H MR spectroscopic imaging – correlation with pathologic findings. Radiology. 2008;246(2):480–8.
21. Charles-Edwards EM, Messiou C, Morgan VA, De Silva SS, McWhinney NA, Katesmark M, et al. Diffusion-weighted imaging in cervical cancer with an endovaginal technique: potential value for improving tumor detection in stage Ia and Ib1 disease. Radiology. 2008;249(2):541–50.
22. de Souza NM, Riches SF, Vanas NJ, Morgan VA, Ashley SA, Fisher C, et al. Diffusion-weighted magnetic resonance imaging: a potential non-invasive marker of tumour aggressiveness in localized prostate cancer. Clin Radiol. 2008;63(7):774–82.
23. Goyal A, Sharma R, Bhalla AS, Gamanagatti S, Seth A, Iyer VK, et al. Diffusion-weighted MRI in renal cell carcinoma: a surrogate marker for predicting nuclear grade and histological subtype. Acta Radiol. 2012;53(3):349–58.
24. Payne GS, Schmidt M, Morgan VA, Giles S, Bridges J, Ind T, et al. Evaluation of magnetic resonance diffusion and spectroscopy measurements as predictive biomarkers in stage 1 cervical cancer. Gynecol Oncol. 2010;116(2):246–52.
25. Zhang Y, Chen JY, Xie CM, Mo YX, Liu XW, Liu Y, et al. Diffusion-weighted magnetic resonance imaging for prediction of response of advanced cervical cancer to chemoradiation. J Comput Assist Tomogr. 2011;35(1):102–7.
26. Wybranski C, Zeile M, Löwenthal D, Fischbach F, Pech M, Röhl FW, et al. Value of diffusion weighted MR imaging as an early surrogate parameter for evaluation of tumor response to high-dose-rate brachytherapy of colorectal liver metastases. Radiat Oncol. 2011;6(1):43.
27. Elmi A, Hedgire SS, Covarrubias D, Abtahi SM, Hahn PF, Harisinghani M. Apparent diffusion coefficient as a non-invasive predictor of treatment response and recurrence in locally advanced rectal cancer. Clin Radiol. 2013;68(10):e524–31.
28. Nakamura K, Imafuku N, Nishida T, Niwa I, Joja I, Hongo A, et al. Measurement of the minimum apparent diffusion coefficient (ADCmin) of the primary tumor and CA125 are predictive of disease recurrence for patients with endometrial cancer. Gynecol Oncol. 2012;124(2):335–9.
29. Park SY, Kim CK, Park BK, Lee HM, Lee KS. Prediction of biochemical recurrence following radical prostatectomy in men with prostate cancer by diffusion-weighted magnetic resonance imaging: initial results. Eur Radiol. 2011;21(5):1111–8.
30. Giles SL, Messiou C, Collins DJ, Morgan VA, Simpkin CJ, West S, et al. Whole-body diffusion-weighted MR imaging for assessment of treatment response in myeloma. Radiology. 2014;271(3):785–94.
31. Blackledge MD, Collins DJ, Tunariu N, Orton MR, Padhani AR, Leach MO, et al. Assessment of treatment response by total tumor volume and global apparent diffusion coefficient using diffusion-weighted MRI in patients with metastatic bone disease: a feasibility study. PLoS One. 2014;9(4):e91779.
32. Malyarenko D, Galban CJ, Londy FJ, Meyer CR, Johnson TD, Rehemtulla A, et al. Multi-system repeatability and reproducibility of apparent diffusion coefficient measurement using an ice-water phantom. J Magn Reson Imaging. 2013;37:1238–46.
33. Wakefield JC, Kyriazi S, Winfield JM, Morgan VA, et al. Diffusion-weighted MRI of advanced ovarian cancer: evaluation of the variability of overall disease burden assessment methods. In: Proceedings of the International Society for Magnetic Resonance in Medicine, 2014; poster presentation no. 553.
34. Waterton JC, Pylkkanen L. Qualification of imaging biomarkers in oncology drug development. Eur J Cancer. 2012;48:409–15.
35. Wolff SD, Balaban RS. Magnetization transfer contrast (MTC) and tissue water proton relaxation in vivo. Magn Reson Med. 1989;10: 135–44.
36. Wolff SD, Balaban RS. Magnetization transfer imaging: practical aspects and clinical applications. Radiology. 1994;192:593–9.
37. Henkelman RM, Stanisz GJ, Graham SJ. Magnetization transfer in MRI: a review. NMR Biomed. 2001;14:57–64.
38. Barker GJ, Tofts PS, Gass A. An interleaved sequence for accurate and reproducible clinical measurement of magnetization transfer ratio. Magn Reson Imaging. 1996;14(4):403–11.
39. Li W, Zhang Z, Nicolai J, Yang G-Y, Omary RA, Larson AC. Magnetization transfer MRI in pancreatic cancer xenograft models. Magn Reson Med. 2012;68:1291–7.
40. Lundbom N. Determination of magnetization transfer contrast in tissue: an MR imaging study of brain tumours. AJR Am J Roentgenol. 1992;159(6):1279–85.
41. Kurki T, Lundbom N, Kalimo H, Valtonen S. MR classification of brain gliomas: value of magnetization transfer and conventional imaging. Magn Reson Imaging. 1995;13:501–11.
42. Sormani MP, Iannucci G, Rocca MA, Mastronardo G, Cercignani M, Miniucci L, et al. Reproducibility of magnetization transfer ratio histogram-derived measures of the brain in healthy volunteers. AJNR Am J Neuroradiol. 2000;21:133–6.
43. Pui MH. Magnetization transfer analysis of brain tumour, infection, and infarction. J Magn Reson Imaging. 2000;12:395–9.
44. Bonini RH, Zeotti D, Saraiva LA, Trad CS, Filho JM, Carrara HH, et al. Magnetization transfer ratio as a predictor of malignancy in breast lesions: preliminary results. Magn Reson Med. 2008;59: 1030–4.
45. Takashima S, Wang J, Takayama F, Momose M, Kawakami A, Saito A, et al. Parotid masses: prediction of malignancy using magnetization transfer and MR imaging findings. AJR Am J Roentgenol. 2001;176:1577–84.
46. Arnold JF, Kotas M, Pyzalski RW, Pracht ED, Flentje M, Jakob PM. Potential of magnetization transfer MRI for target volume definition in patients with non-small-cell lung cancer. J Magn Reson Imaging. 2008;28:1417–24.
47. Martens MH, Lambregts DM, Papanikolaou N, Heijnen LA, Riedl RG, Zur Hausen A, et al. Magnetization transfer ratio: a potential biomarker for the assessment of postradiation fibrosis in patients with rectal cancer. Invest Radiol. 2014;49(1):29–34.
48. Hajnal JV, Baudouin CJ, Oatridge A, Young IR, Bydder GM. Design and implementation of magnetization transfer pulse sequences for clinical use. J Comput Assist Tomogr. 1992;16:7–18.

49. Bottomley PA, Hardy CJ, Argersinger RE, Allen-Moore G. A review of 1H nuclear magnetic resonance relaxation in pathology: are T1 and T2 diagnostic? Med Phys. 1987;14(1):1–37.
50. O'Connor JP, Jackson A, Parker GJ, Roberts C, Jayson GC. Dynamic contrast-enhanced MRI in clinical trials of antivascular therapies. Nat Rev Clin Oncol. 2012;9:167–77.
51. Weidensteiner C, Allegrini PR, Sticker-Jantscheff M, Romanet V, Ferretti S, McSheehy PM. Tumour T1 changes in vivo are highly predictive of response to chemotherapy and reflect the number of viable tumour cells – a preclinical study in mice. BMC Cancer. 2014;14:88.
52. Crawley AP, Henkelman RM. A comparison of one-shot and recovery methods in T1 imaging. Magn Reson Med. 1988;7:23–34.
53. Fram EK, Herfkens RJ, Johnson GA, Glover GH, Karis JP, Shimakawa A, et al. Rapid calculation of T1 using variable flip angle gradient refocused imaging. Magn Reson Imaging. 1987;5(3):201–8.
54. Wang HZ, Riederer SJ, Lee JN. Optimizing the precision in T1 relaxation estimation using limited flip angles. Magn Reson Med. 1987;5:399–416.
55. Leach MO, Brindle KM, Evelhoch JL, Griffiths JR, Horsman MR, Jackson A, et al. The assessment of antiangiogenic and antivascular therapies in early-stage clinical trials using magnetic resonance imaging: issues and recommendations. Br J Cancer. 2005;92:1599–610.
56. Jamin Y, Tucker ER, Poon E, Popov S, Vaughan L, Boult JKR, et al. Evaluation of clinically translatable MR imaging biomarkers of therapeutic response in the TH-MYCN transgenic mouse model of neuroblastoma. Radiology. 2013;266(1):130–40.
57. McSheehy PMJ, Weidensteiner C, Cannet C, Ferretti S, Laurent D, Ruetz S, et al. Quantified tumor T1 is a generic early-response imaging biomarker for chemotherapy reflecting cell viability. Clin Cancer Res. 2010;16(1):212–25.
58. O'Connor JP, Carano RA, Clamp AR, Ross J, Ho CC, Jackson A, et al. Quantifying antivascular effects of monoclonal antibodies to vascular endothelial growth factor: insights from imaging. Clin Cancer Res. 2009;15(21):6674–82.
59. Jensen KE, Sørensen PG, Thomsen C, Christoffersen P, Henriksen O, Karle H. Magnetic resonance imaging of the bone marrow in patients with acute leukemia during and after chemotherapy. Acta Radiol. 1990;31:361–9.
60. Sourbron SP, Buckley DL. Classic models for dynamic contrast-enhanced MRI. NMR Biomed. 2013;26(8):1004–27.
61. Jackson A, O'Connor JP, Parker GJ, Jayson GC. Imaging tumor vascular heterogeneity and angiogenesis using dynamic contrast-enhanced magnetic resonance imaging. Clin Cancer Res. 2007;13(12):3449–59.
62. Li SP, Padhani AR. Tumor response assessments with diffusion and perfusion MRI. J Magn Reson Imaging. 2012;35(4):745–63.
63. Tofts PS. Modeling tracer kinetics in dynamic Gd-DTPA MR imaging. J Magn Reson Imaging. 1997;7(1):91–101.
64. Tofts PS, Brix G, Buckley DL, Evelhoch JL, Henderson E, Knopp MV, et al. Estimating kinetic parameters from dynamic contrast-enhanced T1-weighted MRI of a diffusable tracer: standardized quantities and symbols. J Magn Reson Imaging. 1999;10(3):223–32.
65. Lankester KJ, Taylor JN, Stirling JJ, Boxall J, D'Arcy JA, Collins DJ, et al. Dynamic MRI for imaging tumor microvasculature: comparison of susceptibility and relaxivity techniques in pelvic tumors. J Magn Reson Imaging. 2007;25:796–805.
66. Messiou C, Orton M, Ang JE, Collins DJ, Morgan VA, Mears D, et al. Advanced solid tumors treated with cediranib: comparison of dynamic contrast-enhanced MR imaging and CT as markers of vascular activity. Radiology. 2012;265(2):426–36.
67. O'Connor JP, Jackson A, Parker GJ, Jayson GC. DCE-MRI biomarkers in the clinical evaluation of antiangiogenic and vascular disrupting agents. Br J Cancer. 2007;96(2):189–95.
68. Ciunci CA, Perini RF, Avadhani AN, Kang HC, Sun W, Redlinger M, et al. Phase 1 and pharmacodynamic trial of everolimus in combination with cetuximab in patients with advanced cancer. Cancer. 2014;120(1):77–85.
69. Yap TA, Olmos D, Brunetto AT, Tunariu N, Barriuso J, Riisnaes R, et al. Phase I trial of a selective c-MET inhibitor ARQ 197 incorporating proof of mechanism pharmacodynamic studies. J Clin Oncol. 2011;29(10):1271–9.
70. Nathan P, Zweifel M, Padhani AR, Koh DM, Ng M, Collins DJ, et al. Phase I trial of combretastatin A4 phosphate (CA4P) in combination with bevacizumab in patients with advanced cancer. Clin Cancer Res. 2012;18(12):3428–39.
71. Glade Bender JL, Lee A, Reid JM, Baruchel S, Roberts T, Voss SD, et al. Phase I pharmacokinetic and pharmacodynamic study of pazopanib in children with soft tissue sarcoma and other refractory solid tumors: a children's oncology group phase I consortium report. J Clin Oncol. 2013;31(24):3034–43.
72. Hsu CY, Shen YC, Yu CW, Hsu C, Hu FC, Hsu CH, et al. Dynamic contrast-enhanced magnetic resonance imaging biomarkers predict survival and response in hepatocellular carcinoma patients treated with sorafenib and metronomic tegafur/uracil. J Hepatol. 2011;55(4):858–65.
73. Jarnagin WR, Schwartz LH, Gultekin DH, Gönen M, Haviland D, Shia J, et al. Regional chemotherapy for unresectable primary liver cancer: results of a phase II clinical trial and assessment of DCE-MRI as a biomarker of survival. Ann Oncol. 2009;20(9):1589–95.
74. Shih TT, Hou HA, Liu CY, Chen BB, Tang JL, Chen HY, et al. Bone marrow angiogenesis magnetic resonance imaging in patients with acute myeloid leukemia: peak enhancement ratio is an independent predictor for overall survival. Blood. 2009;113(14):3161–7.
75. Pickles MD, Manton DJ, Lowry M, Turnbull LW. Prognostic value of pre-treatment DCE-MRI parameters in predicting disease free and overall survival for breast cancer patients undergoing neoadjuvant chemotherapy. Eur J Radiol. 2009;71(3):498–505.
76. Flaherty KT, Rosen MA, Heitjan DF, Gallagher ML, Schwartz B, Schnall MD, et al. Pilot study of DCE-MRI to predict progression-free survival with sorafenib therapy in renal cell carcinoma. Cancer Biol Ther. 2008;7(4):496–501.
77. Miles KA, Lee T-Y, Goh V, Klotz E, Cuenod C, Bisdas S, et al. Current status and guidelines for the assessment of tumour vascular support with dynamic contrast-enhanced computed tomography. Eur Radiol. 2012;22(7):1430–41.
78. Ng CS, Waterton JC, Kundra V, Brammer D, Ravoori M, Han L, et al. Reproducibility and comparison of DCE-MRI and DCE-CT perfusion parameters in a rat tumor model. Technol Cancer Res Treat. 2012;11(3):279–88.
79. Driscoll B, Keller H, Jaffray D, Coolens C. Development of a dynamic quality assurance testing protocol for multisite clinical trial DCE-CT accreditation. Med Phys. 2013;40(8):081906.
80. Mandeville HC, Ng QS, Daley FM, Barber PR, Pierce G, Finch J, et al. Operable non-small cell lung cancer: correlation of volumetric helical dynamic contrast-enhanced CT parameters with immunohistochemical markers of tumor hypoxia. Radiology. 2012;264(2):581–9.
81. Chen Y, Zhang J, Dai J, Feng X, Lu H, Zhou C. Angiogenesis of renal cell carcinoma: perfusion CT findings. Abdom Imaging. 2012;35(5):622–8.
82. Goh V, Glynne-Jones R. Perfusion CT imaging of colorectal cancer. Br J Radiol. 2014;87:20130811.
83. Lind JS, Meijerink MR, Dingemans AM, van Kuijk C, Ollers MC, de Ruysscher D, et al. Dynamic contrast-enhanced CT in patients treated with sorafenib and erlotinib for non-small cell lung cancer: a new method of monitoring treatment? Eur Radiol. 2010;20(12):2890–8.
84. Okada H, Hontsu S, Miura S, Asakawa I, Tamamoto T, Katayama E, et al. Changes of tumor size and tumor contrast enhancement

during radiotherapy for non-small-cell lung cancer may be suggestive of treatment response. J Radiat Res. 2012;53(2):326–32.
85. Lim WT, Ng QS, Ivy P, Leong SS, Singh O, Chowbay B, et al. A phase II study of pazopanib in Asian patients with recurrent/metastatic nasopharyngeal carcinoma. Clin Cancer Res. 2011;17(16):5481–9.
86. Tofts PS, Collins DJ. Multicentre imaging measurements for oncology and in the brain. Br J Radiol. 2011;84:S213–26.
87. Padhani A. Science to practice: what does MR oxygenation imaging tell us about human breast cancer hypoxia? Radiology. 2010;254(1):1–3.
88. McPhail LD, Robinson SP. Intrinsic susceptibility MR imaging of chemically induced rat mammary tumors: relationship to histologic assessment of hypoxia and fibrosis. Radiology. 2010;254(1):110–8.
89. Baker LC, Boult JK, Jamin Y, Gilmour LD, Walker-Samuel S, Burrell JS, et al. Evaluation and immunohistochemical qualification of carbogen-induced ΔR2* as a noninvasive imaging biomarker of improved tumor oxygenation. Int J Radiat Oncol Biol Phys. 2013;87(1):160–7.
90. Jamin Y, Glass L, Hallsworth A, George R, Koh D-M, Pearson AD, et al. Intrinsic susceptibility MRI identifies tumors with ALK-F1174L mutation in genetically-engineered murine models of high-risk neuroblastoma. PLoS One. 2014;9(3):e92886.
91. Rodrigues LM, Howe FA, Griffiths JR, Robinson SP. Tumor R2* is a prognostic indicator of acute radiotherapeutic response in rodent tumors. J Magn Reson Imaging. 2004;19:482–8.
92. Bradley DP, Tessier JJ, Ashton SE, Waterton JC, Wilson Z, Worthington PL, et al. Correlation of MRI biomarkers with tumor necrosis in Hras5 tumor xenograft in athymic rats. Neoplasia. 2007;9(5):382–91.
93. Li SP, Taylor NJ, Makris A, Ah-See M-LW, Beresford MJ, Stirling JJ, et al. Primary human breast adenocarcinoma: imaging and histologic correlates of intrinsic susceptibility-weighted MR imaging before and during chemotherapy. Radiology. 2010;257(3):643–52.
94. Chopra S, Foltz WD, Milosevic MF, Toi A, Bristow RG, Menard C, et al. Comparing oxygen-sensitive MRI (BOLD R2*) with oxygen electrode measurements: a pilot study in men with prostate cancer. Int J Radiat Biol. 2009;85(9):805–13.
95. Jhaveri KS, Cleary SP, Fischer S, Haider MA, Pargoankar V, Khalidi K, et al. Blood oxygen level-dependent liver MRI: can It predict microvascular invasion in HCC? J Magn Reson Imaging. 2013;37:692–9.
96. Dennie J, Mandeville JB, Boxerman JL, Packard SD, Rosen BR, Weisskoff RM. NMR imaging of changes in vascular morphology due to tumor angiogenesis. Magn Reson Med. 1998;40(6):793–9.
97. Tropres I, Grimault S, Vaeth A, Grillon E, Julien C, Payen J-F, et al. Vessel size imaging. Magn Reson Med. 2001;45(3):397–408.
98. Kiselev VG, Strecker R, Ziyeh S, Hennig J. Vessel size imaging in humans. Magn Reson Med. 2005;53:553–63.
99. Schmainda KM, Rand SD, Joseph AM, Lund R, Ward BD, Pathak AP, et al. Characterization of a first-pass gradient-echo spin-echo method to predict brain tumor grade and angiogenesis. AJNR Am J Neuroradiol. 2004;25(9):1524–32.
100. Batchelor TT, Sorensen AG, di Tomaso E, Zhang W-T, Duda DG, Cohen KS, et al. AZD2171, a pan-VEGF receptor tyrosine kinase inhibitor, normalizes tumor vasculature and alleviates edema in glioblastoma patients. Cancer Cell. 2007;11:83–95.
101. Pannetier N, Lemasson B, Christen T, Tachrount M, Tropres I, Farion R, et al. Vessel size index measurements in a rat model of glioma: comparison of the dynamic (Gd) and steady-state (iron-oxide) susceptibility contrast MRI approaches. NMR Biomed. 2012;25(2):218–26.
102. Valable S, Lemasson B, Farion R, Beaumont M, Segebarth C, Remy C, et al. Assessment of blood volume, vessel size, and the expression of angiogenic factors in two rat glioma models: a longitudinal in vivo and ex vivo study. NMR Biomed. 2008;21(10):1043–56.
103. Douma K, Oostendorp M, Slaaf DW, Post MJ, Backes WH, van Zandvoort MA. Evaluation of magnetic resonance vessel size imaging by two-photon laser scanning microscopy. Magn Reson Med. 2010;63(4):930–9.
104. Persigehl T, Ring J, Budny T, Hahnenkamp A, Stoeppeler S, Schwartz LH, et al. Vessel size imaging (VSI) by robust magnetic resonance (MR) relaxometry MR-VSI of solid tumours in correlation with immunohistology and intravital microscopy. Mol Imaging. 2013;12(7):1–11.
105. Kim E, Cebulla J, Ward BD, Rhie K, Zhang J, Pathak AP. Assessing breast cancer angiogenesis in vivo: which susceptibility contrast MRI biomarkers are relevant? Magn Reson Med. 2013;70(4):1106–16.
106. Burrell JS, Bradley RS, Walker-Samuel S, Jamin Y, Baker LC, Boult JK, et al. MRI measurements of vessel caliber in tumour xenografts: comparison with vascular corrosion casting. Microvasc Res. 2012;84(3):323–9.
107. Lemasson B, Christen T, Tizon X, Farion R, Fondraz N, Provent P, et al. Assessment of multiparametric MRI in a human glioma model to monitor cytotoxic and anti-angiogenic drug effects. NMR Biomed. 2011;24(5):473–82.
108. Sampath D, Oeh J, Wyatt SK, Cao TC, Koeppen H, Eastham-Anderson J, et al. Multimodal microvascular imaging reveals that selective inhibition of class I PI3K is sufficient to induce an antivascular response. Neoplasia. 2013;15(7):694–711.
109. Walker-Samuel S, Boult JK, McPhail LD, Box G, Eccles SA, Robinson SP. Non-invasive in vivo imaging of vessel calibre in orthotopic prostate tumour xenografts. Int J Cancer. 2012;130:1284–93.
110. Gahramanov S, Muldoon LL, Varallyay CG, Li X, Kraemer DF, Fu R, et al. Pseudoprogression of glioblastoma after chemo- and radiation therapy: diagnosis by using dynamic susceptibility-weighted contrast-enhanced perfusion MR imaging with ferumoxytol versus gadoteriol and correlation with survival. Radiology. 2013;266(3):842–52.
111. Gambarota G, van Laarhoven HW, Philippens M, Lok J, van der Kogel A, Punt CJ, et al. Assessment of absolute blood volume in carcinoma by USPIO contrast-enhanced MRI. Magn Reson Imaging. 2006;24(3):279–86.
112. Law M, Yang S, Wang H, Babb JS, Johnson G, Cha S, et al. Glioma grading: sensitivity, specificity, and predictive values of perfusion MR imaging and proton MR spectroscopic imaging compared with conventional MR imaging. AJNR Am J Neuroradiol. 2003;24(10):1989–98.
113. Barajas RF, Chang JS, Segal MR, Parsa AT, McDermott MW, Berger MS, et al. Differentiation of recurrent glioblastoma multiforme from radiation necrosis after external beam radiation therapy with dynamic susceptibility-weighted contrast-enhanced perfusion MR imaging. Radiology. 2009;253(2):486–96.
114. Law M, Young RJ, Babb JS, Peccerelli N, Chheang S, Gruber ML, et al. Gliomas: predicting time to progression or survival with cerebral blood volume measurements at dynamic susceptibility-weighted contrast-enhanced perfusion MR imaging. Radiology. 2008;247(2):490–8.
115. O'Connor JP, Jayson GC. Do imaging biomarkers relate to outcome in patients treated with VEGF inhibitors? Clin Cancer Res. 2012;18(24):6588–98.
116. Desar IM, ter Voert EG, Hambrock T, van Asten JJ, van Spronsen DJ, Mulders PF, et al. Functional MRI techniques demonstrate early vascular changes in renal cell cancer patients treated with sunitinib: a pilot study. Cancer Imaging. 2011;11(1):259–65.
117. Ah-See M-LW, Makris A, Taylor NJ, Harrison M, Richman PI, Burcombe RJ, et al. Early changes in functional dynamic magnetic resonance imaging predict for pathologic response to neoadjuvant chemotherapy in primary breast cancer. Clin Cancer Res. 2008;14(20):6580–9.

118. Alonzi R, Padhani AR, Taylor NJ, Collins DJ, D'Arcy JA, Stirling JJ, et al. Antivascular effects of neoadjuvant androgen deprivation for prostate cancer: an in vivo human study using susceptibility and relaxivity dynamic MRI. Int J Radiat Oncol Biol Phys. 2011;80(3):721–7.
119. de Graaf RA. In vivo NMR spectroscopy. 2nd ed. Chichester: Wiley; 2007.
120. Provencher SW. Estimation of metabolite concentrations from localized NMR spectra. Magn Reson Med. 1993;30(6):672–9.
121. Provencher SW. Automatic quantitation of localized in vivo 1H spectra with LCModel. NMR Biomed. 2001;14(4):260–4.
122. jMRUI. MRUI: Magnetic Resonance User Interface. http://www.mrui.uab.es/mrui/. Accessed 3 January 2015.
123. Vanhamme L, van den Boogaart A, Van Huffel S. Improved method for accurate and efficient quantification of MRS data with use of prior knowledge. J Magn Reson. 1997;129(1):35–43.
124. Naressi A, Couturier C, Devos JM, Janssen M, Mangeat C, de Beer R, et al. Java-based graphical user interface for the MRUI quantitation package. MAGMA. 2001;12(2-3):141–52.
125. Warburg O. On the origin of cancer cells. Science. 1956;123(3191):309–14.
126. Howe FA, Barton SJ, Cudlip SA, Stubbs M, Saunders DE, Murphy M, et al. Metabolic profiles of human brain tumors using quantitative in vivo 1H magnetic resonance spectroscopy. Magn Reson Med. 2003;49(2):223–32.
127. Nelson SJ, Graves E, Pirzkall A, Li X, Chan AA, Vigneron DB, et al. In vivo molecular imaging for planning radiation therapy of gliomas: an application of 1H MRSI. J Magn Reson Imaging. 2002;16(4):464–76.
128. Begley JK, Redpath TW, Bolan PJ, Gilbert FJ. In vivo proton magnetic resonance spectroscopy of breast cancer: a review of the literature. Breast Cancer Res. 2012;14(2):207.
129. Kurhanewicz J, Vigneron D, Carroll P, Coakley F. Multiparametric magnetic resonance imaging in prostate cancer: present and future. Curr Opinion Urol. 2008;18(1):71–7.
130. Griffin JL, Shockcor JP. Metabolic profiles of cancer cells. Nat Rev Cancer. 2004;4(7):551–61.
131. Boren J, Brindle KM. Apoptosis-induced mitochondrial dysfunction causes cytoplasmic lipid droplet formation. Cell Death Differ. 2012;19(9):1561–70.
132. Glaholm J, Leach MO, Collins DJ, Mansi J, Sharp JC, Madden A, et al. In-vivo 31P magnetic resonance spectroscopy for monitoring treatment response in breast cancer. Lancet. 1989;1(8650):1326–7.
133. Negendank W. Studies of human tumors by MRS: a review. NMR Biomed. 1992;5(5):303–24.
134. Arias-Mendoza F, Payne GS, Zakian K, Stubbs M, O'Connor OA, Mojahed H, et al. Noninvasive phosphorus magnetic resonance spectroscopic imaging predicts outcome to first-line chemotherapy in newly diagnosed patients with diffuse large B-cell lymphoma. Acad Radiol. 2013;20(9):1122–9.
135. Moon RB, Richards JH. Determination of intracellular pH by 31P magnetic resonance. J Biol Chem. 1973;248(20):7276–8.
136. Graham RA, Taylor AH, Brown TR. A method for calculating the distribution of pH in tissues and a new source of pH error from the 31P-NMR spectrum. Am J Physiol. 1994;266(2 Pt 2):R638–45.
137. Stubbs M, McSheehy PM, Griffiths JR, Bashford CL. Causes and consequences of tumour acidity and implications for treatment. Mol Med Today. 2000;6(1):15–9.
138. Sonveaux P, Végran F, Schroeder T, Wergin MC, Verrax J, Rabbani ZN, et al. Targeting lactate-fueled respiration selectively kills hypoxic tumor cells in mice. J Clin Invest. 2008;118(12):3930–42.
139. McSheehy PM, Griffiths JR. 19F MRS studies of fluoropyrimidine chemotherapy. a review. NMR Biomed. 1989;2(4):133–41.
140. Mason RP, Rodbumrung W, Antich PP. Hexafluorobenzene: a sensitive 19F NMR indicator of tumor oxygenation. NMR Biomed. 1996;9(3):125–34.
141. Lee CP, Payne GS, Oregioni A, Ruddle R, Tan S, Raynaud FI, et al. A phase I study of the nitroimidazole hypoxia marker SR4554 using 19F magnetic resonance spectroscopy. Br J Cancer. 2009;101(11):1860–8.
142. Nelson SJ, Kurhanewicz J, Vigneron DB, Larson PE, Harzstark AL, Ferrone M, et al. Metabolic imaging of patients with prostate cancer using hyperpolarized 000[1-13C] pyruvate. Sci Transl Med. 2013;5(198):198ra108.